



Tidal flow over three-dimensional topography generates out-of-forcing-plane harmonics

Benjamin King,¹ H. P. Zhang,¹ and Harry L. Swinney¹

Received 10 March 2010; revised 30 April 2010; accepted 18 May 2010; published 29 July 2010.

[1] We conduct laboratory experiments and direct numerical simulations on internal gravity waves generated by tidal flow over a model three-dimensional Gaussian mountain on the sea floor. When $2\omega < N$ (where ω is the tidal frequency and N is the buoyancy frequency), the flow generates second harmonic internal waves that propagate perpendicular to the tidal forcing direction. These unexpected harmonics are observed only when the maximum slope of the bottom topography is greater than the slope of internal wave propagation. The out-of-plane harmonics saturate at a higher tidal forcing amplitude than the normal in-tidal-forcing-plane harmonics, and could lead to increased wave breaking and mixing near rough topography in the ocean. **Citation:** King, B., H. P. Zhang, and H. L. Swinney (2010), Tidal flow over three-dimensional topography generates out-of-forcing-plane harmonics, *Geophys. Res. Lett.*, 37, L14606, doi:10.1029/2010GL043221.

1. Introduction

1.1. Background

[2] The global thermohaline circulation is maintained by roughly 2 TW of mixing energy, about half of which is extracted from the barotropic tide [Munk and Wunsch, 1998; Egbert and Ray, 2000]. The transfer of this barotropic energy from large to small length scales requires a series of processes [Jayne *et al.*, 2004], the first step being energy conversion from the barotropic to the baroclinic tide. The generation of internal waves by tidal flow over two-dimensional (2D) topography has been studied recently by Khatiwala [2003], Petrelis *et al.* [2006], Zhang *et al.* [2007], Peacock *et al.* [2008], and Balmforth and Peacock [2009]. Some studies have also examined internal wave generation by tidal flow past three-dimensional (3D) topography. Holloway and Merrifield [1999] and Munroe and Lamb [2005] studied the internal tides generated by 3D Gaussian mountains with varying horizontal aspect ratios (defined as the longer to the shorter horizontal dimension). Baines [2007] studied tidal flow past a pillbox. Flynn *et al.* [2003] used a vertically oscillating sphere to study the generation of internal waves by supercritical topography (topography is supercritical when the maximum slope of the topography is greater than the slope of internal wave propagation). Expanding on this work, King *et al.* [2009] performed laboratory experiments and numerical simulations of a horizontally oscillating (tidal) flow over a half-sphere on a plane, verifying the linear inviscid theory of

Appleby and Crighton [1987] for small tidal excursion parameter ϵ (defined as the ratio of barotropic tidal amplitude to a characteristic horizontal length scale of the topography). For larger excursion parameters, although the internal tide was still found to be more concentrated in the tidal forcing direction, 3D effects were found to be important. Notably, King *et al.* [2009] observed a nonlinear boundary flow oscillating at twice the tidal forcing frequency ω . Parameters were chosen such that $2\omega > N$ (with Coriolis parameter $f=0$) and second harmonic internal waves were not allowed by the dispersion relation

$$\frac{\omega}{N} = \sin\theta, \quad (1)$$

where θ is the angle of internal tide propagation measured from the horizontal, and N is the buoyancy frequency, $N = \sqrt{-(g/\rho(z))(d\rho/dz)}$, with g the gravitational acceleration and $\rho(z)$ the density as a function of depth. In this parameter regime, the nonlinear boundary flow resulted in a large scale horizontal circulation near the topography.

1.2. Present Study

[3] We examine tidal flow past 3D topography for the case $2\omega < N$, and we find the boundary flow generates second harmonic internal tides that propagate away from the topography in the direction perpendicular to the tidal forcing. We make the simplifying assumption that the Coriolis parameter $f=0$. The model system is an axisymmetric Gaussian mountain of height 7 cm and $1/e$ half-width $\sigma = 2.85$ cm (cf. Figure 1a). This model geometry is chosen so that the maximum topographic slope is greater than the slope of both fundamental and second harmonic internal tide propagation. Two additional model topographic slopes (discussed in Section 3.2) are utilized to determine the effect of varying topographic slope on second harmonic generation. In this study, the buoyancy frequency $N = 1.5$ rad/s is independent of depth and the tidal forcing frequency $\omega = 0.6$ rad/s. Inserting these values into (1) gives propagation angles of 23.6° for the fundamental internal tides at the tidal forcing frequency ω and 53.1° for second harmonic internal tides at 2ω .

[4] This paper is organized as follows: Section 2 presents the numerical and experimental methods. Section 3 discusses the dependence of the second harmonic internal tides on tidal forcing amplitude and topographic slope, and summarizes calculations of energy flux associated with the internal tides. Section 4 discusses how the results contribute to the understanding of the generation of internal tides.

2. Methods

[5] Our numerical simulations are performed using CDP 2.4, a finite-volume based Large Eddy Simulation (LES)

¹Center for Nonlinear Dynamics and Department of Physics, University of Texas at Austin, Austin, Texas, USA.

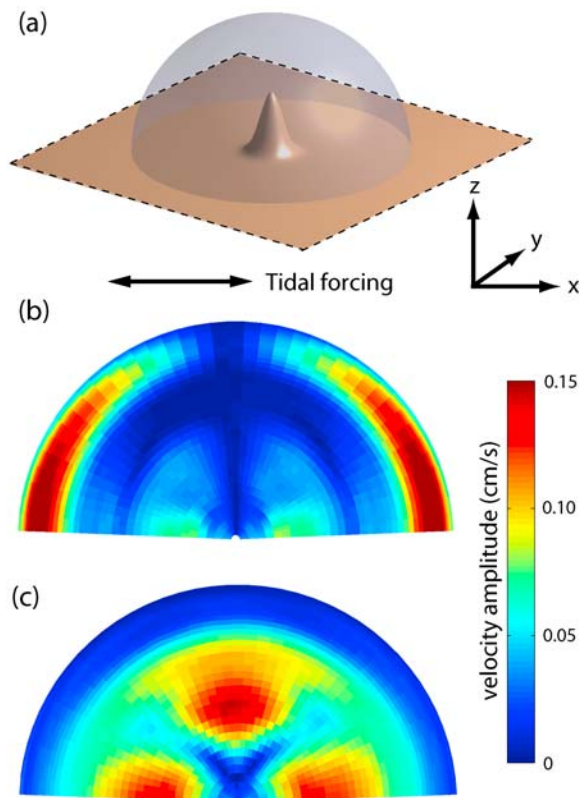


Figure 1. (a) A schematic diagram of the model topography, a 7 cm high Gaussian mountain with 1/e half-width $\sigma = 2.85$ cm. The transparent blue sphere with radius 15 cm is the imaginary visualization surface which is viewed from above (along the positive z -axis) in Figures 1b and 1c. (b) Fundamental and (c) second harmonic wave velocity amplitudes visualized near the topography for velocity components normal to the spherical surface depicted in Figure 1a. The out-of-forcing-plane second harmonic velocity amplitude in Figure 1c is slightly stronger than the in-plane second harmonics, and is comparable in amplitude to the fundamental wave in Figure 1b. The dimensionless tidal forcing amplitude is $A/\sigma = 0.50$.

code developed by Frank Ham at the Center for Integrated Turbulence Simulations at Stanford University [Ham and Iaccarino, 2004]. We turn off all subgrid-scale modeling, making it a Direct Numerical Simulation (DNS), and modify the code to include buoyancy effects. An oscillatory tidal flow of the form $u(t) = A\omega \sin \omega t$ is enforced at the left and right boundaries; the nondimensional forcing amplitude A/σ is varied between 0.0625 and 1. Due to symmetry about the $y = 0$ plane (the vertical plane containing the tidal forcing direction), computations are run only for half of the domain ($y > 0$). The computational domain is 100 cm long \times 40 cm wide \times 45 cm high. Further details and code verification are discussed by King *et al.* [2009].

[6] Experiments are performed in a glass tank 90 cm long \times 45 cm wide \times 60 cm high. The tank is filled with a linearly stratified salt solution, with the density of the fluid varying from 1.15 g/cm³ at the bottom of the tank to 1.00 g/cm³ (freshwater) at the top.

[7] A three-dimensional Gaussian mountain made from Delrin® is used to simulate bottom topography in the ocean.

The mountain is axisymmetric, with a height of 7 cm and 1/e half-width $\sigma = 2.85$ cm. It is fastened to a horizontal aluminum plate and attached in an inverted position, as by Echeverri *et al.* [2009], to a traverse mechanism above the water surface. The nondimensionalized forcing amplitude is $A/\sigma = 0.25$.

[8] We use Particle Image Velocimetry (PIV) to measure the velocity field in vertical planes through the center of the mountain, both parallel and perpendicular to the tidal forcing direction. (The fields are determined on a 50×50 grid, corresponding to a spatial resolution of 0.28 cm [Zhang *et al.*, 2007; King *et al.*, 2009].) The measurements on the perpendicular plane are more difficult than for the parallel plane because tracer particles oscillating through the perpendicular plane have a short residence time in the light sheet. Nevertheless, we obtain velocity field data perpendicular to the tidal flow that compare reasonably well with the simulation results (see Section 3). Measurements in the parallel plane using a similar laboratory setup show very close correspondence with simulations conducted with the same numerical code [King *et al.*, 2009].

3. Results

[9] The velocity amplitudes $A\omega$ of the internal tides crossing the spherical visualization surface in Figure 1a were obtained by fitting the time series of surface-normal velocity to sinusoidal components at the tidal forcing frequency ω and twice the tidal forcing frequency 2ω . The results for the ω component of the internal tide are shown in Figure 1b, which shows the $\cos \phi$ dependence on the azimuthal angle ϕ expected (for small forcing amplitudes) from the linear inviscid theory of Appleby and Crighton [1987]. Figure 1c shows that in addition to the expected second harmonics in the tidal forcing direction, there is also a second harmonic internal wave generated perpendicular to this direction. We will refer to internal tides in the $y = 0$ plane, which contains the tidal forcing direction, as ‘in-plane’ waves. Internal tides in the $x = 0$ plane, which is perpendicular to the tidal forcing direction, will be referred to as ‘out-of-plane.’ At high tidal forcing amplitude, the unexpected out-of-plane second harmonic wavebeam has amplitude comparable to the internal tides generated at the tidal forcing frequency.

[10] A direct comparison between simulation and experiment is shown in Figures 2a–2d. The comparison is made in the $x = 0$ plane, perpendicular to the forcing direction. For a quantitative comparison, Figures 2c and 2d show velocity profiles for both experiments and simulations at two phases of tidal forcing. The experimental results agree well with the simulations; both show a strong out-of-plane second harmonic wave.

3.1. Dependence of Harmonics on Amplitude

[11] The velocity amplitudes of the in-plane and out-of-plane second harmonic waves determined for tidal forcing amplitudes $0.0625 < A/\sigma < 1$ are shown in Figure 2e. The in-plane and out-of-plane harmonics both scale as the square of the forcing amplitude, as expected for a nonlinear generation process. At low forcing amplitudes, the in-plane harmonics are stronger than the out-of-plane harmonics, but the in-plane harmonics begin to saturate at a smaller forcing amplitude. At $A/\sigma \approx 0.4$, the out-of-plane harmonics become stronger, and at the highest amplitude reported here, $A/\sigma = 1$, the out-of-

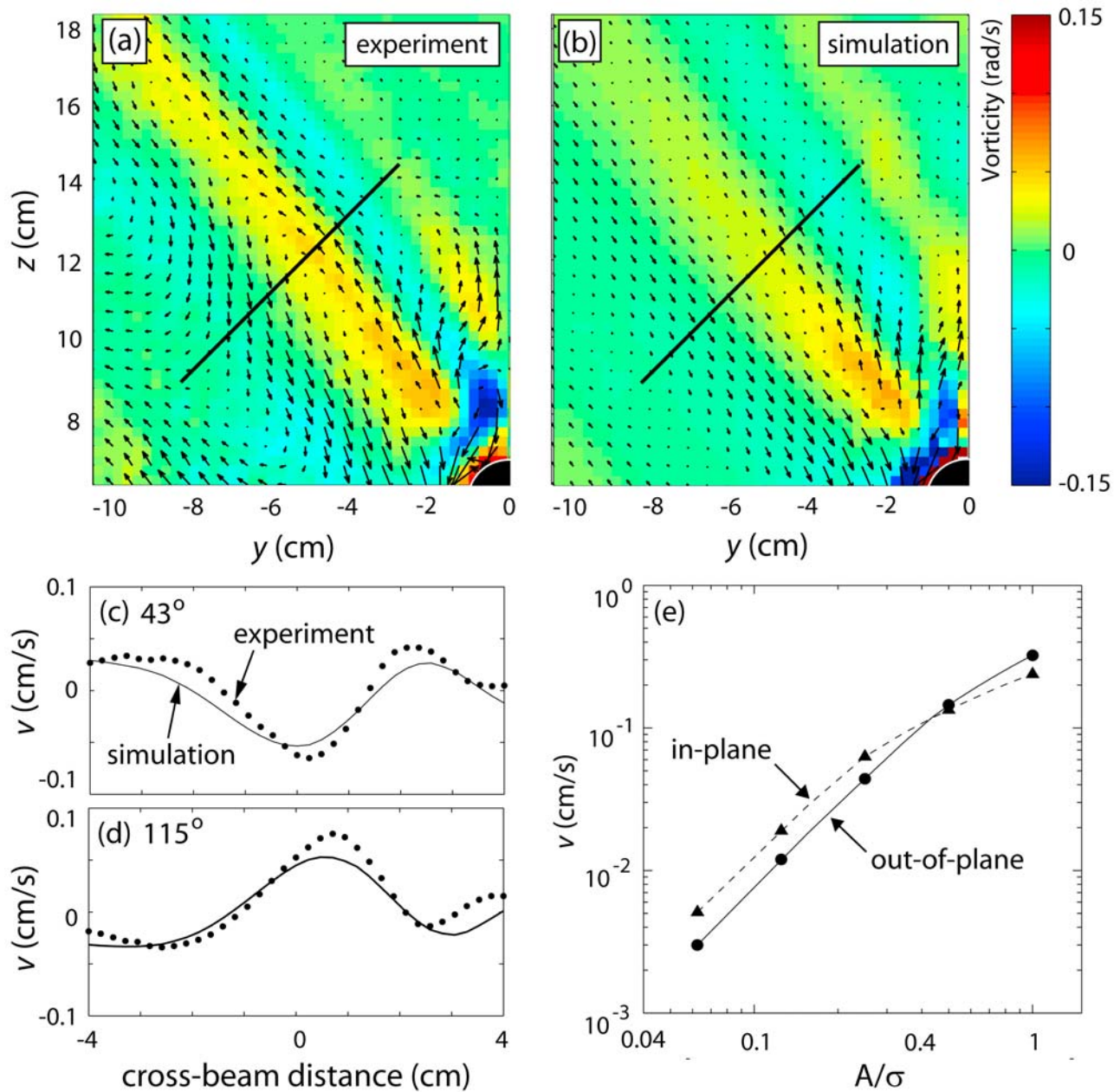


Figure 2. Snapshots of the out-of-plane second harmonics in (a) experiment and (b) simulation ($A/\sigma = 0.25$). The tip of the Gaussian mountain is in the lower right corner. Arrows denote instantaneous velocity, taken when the tidal flow is near its maximum, coming out of the page (phase 90°), and color represents vorticity. (c and d) Velocity profiles at phases 43° and 115° , respectively, along the diagonal lines in Figures 2a and 2b (the velocity component is along the beam direction). (e) Second harmonic velocity amplitude dependence on tidal forcing amplitude at distance $r = 15$ cm from the origin. The in-plane harmonics (triangles) and out-of-plane harmonics (circles) both scale quadratically with forcing amplitude for small forcing, as expected. The in-plane harmonics begin to saturate at lower tidal forcing amplitude than the out-of-plane harmonics.

plane second harmonics have amplitude 36% greater than the in-plane second harmonics.

3.2. Dependence on Topographic Slope

[12] Previous work has examined the effect of topographic steepness on the generation of internal tides [Khaliwala, 2003; Munroe and Lamb, 2005; Balmforth and Peacock, 2009]. The relevant dimensionless parameter is the ratio of

maximum topographic slope to the slope of the generated internal waves. We have conducted numerical simulations for Gaussian mountains with height 7 cm and three different maximum topographic slopes S_{\max} . Using the relation,

$$S = \sqrt{\frac{\omega^2}{N^2 - \omega^2}}, \quad (2)$$

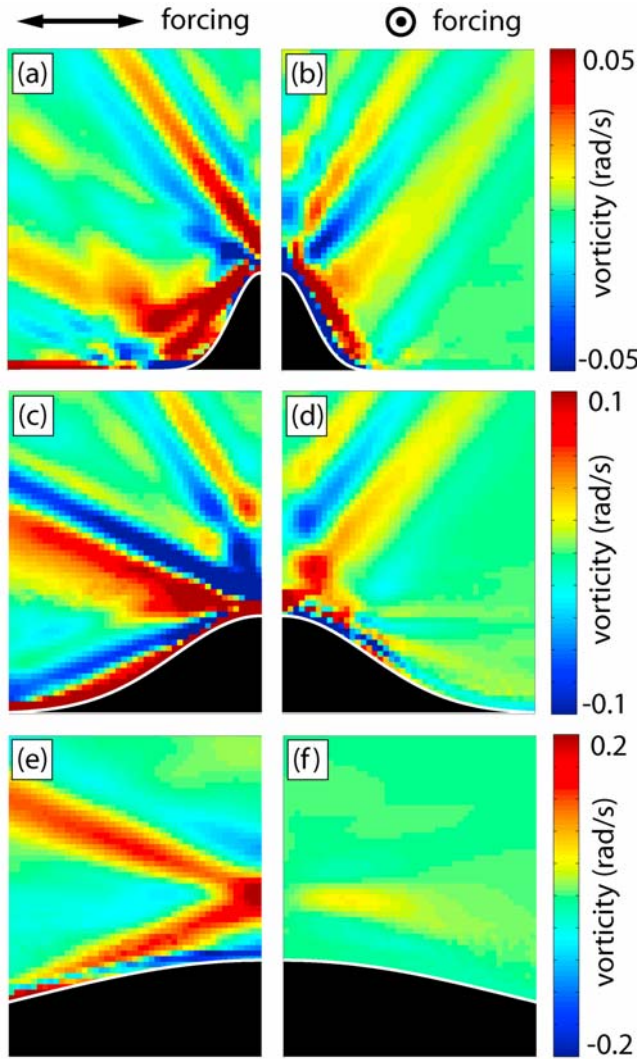


Figure 3. Vorticity snapshots of simulation results in the forcing plane and perpendicular to the forcing plane for (a and b) $S_2 < S_{\max}$ (2ω -supercritical), (c and d) $S_1 < S_{\max} < S_2$ (ω -supercritical), and (e and f) $S_{\max} < S_1$ (subcritical), where $S_1 = 0.436$ and $S_2 = 1.33$ are respectively the slopes of the fundamental and second harmonic, and S_{\max} is the maximum topographic slope (2.11, 0.693, and 0.249 for the 7 cm high mountains with $1/e$ half-widths 2.85 cm, 8.66 cm, and 24.1 cm, respectively). The snapshots are taken when the tidal forcing flow is at its maximum, coming out of the page; note the difference in color bars for the three different topographies. Each plot shows a fluid region 18 cm wide \times 23 cm high.

the three topographic slopes can be compared to the slopes for the fundamental wave S_1 and the second harmonic wave S_2 , as shown in Figure 3, both in the in-plane (Figures 3a, 3c, and 3e) and out-of-plane (Figures 3b, 3d, and 3f) directions. The topography in Figures 3a and 3b is the same as that used in the previous sections of this study. The maximum slope of this topography is greater than the slope of both the fundamental and second harmonic beams (i.e., the topography is 2ω -supercritical), resulting in downward-propagating internal tides at frequencies ω and 2ω , in addition to the normal upward propagating internal tides.

[13] Fundamental waves are absent in the out-of-forcing plane direction, Figure 3b, as expected from linear inviscid theory [Appleby and Crighton, 1987]. Figures 3c and 3d show results for topography with maximum slope greater than S_1 but less than S_2 (ω -supercritical topography). As expected, there are upward and downward propagating fundamental waves but only upward propagating second harmonic waves in the forcing direction (Figure 3c). Second harmonics are also generated in the out-of-forcing plane direction (Figure 3d), but they only propagate upward, unlike the harmonics on the (2ω -supercritical topography (Figure 3b), which has upward and downward propagating second harmonics.

[14] Figures 3e and 3f show topography with maximum topographic slope less than both S_1 and S_2 (subcritical topography). In this case, waves at the tidal forcing frequency occur only in the forcing direction, and internal tides are absent in the out-of-forcing plane direction. As expected, more of the barotropic tide is converted to internal tides for the wider Gaussian mountains, as these mountains present a greater obstacle to the tidal flow. In the top two cases, however, the out-of-plane harmonics are comparable in strength to the in-plane harmonics and fundamental wave beams.

3.3. Energy Flux

[15] To determine the internal tidal energy radiated perpendicular to the tidal forcing direction, we first separate the barotropic and baroclinic components of the pressure and velocity. The barotropic components of the pressure and velocity perturbations are obtained from the x -component of the Navier-Stokes equation and are given by:

$$p'_{bt} = -A\omega^2 x \cos \omega t, \quad (3)$$

$$u'_{bt} = A\omega \sin \omega t. \quad (4)$$

Far from the topography, where the barotropic flow can be assumed to be largely unaffected by the presence of the topography, we can subtract the above quantities from the total perturbation pressure and velocities to obtain the baroclinic perturbation quantities, p'_{bc} and u'_{bc} , associated with the internal tides. Integrating across an arbitrary surface for one tidal forcing period gives the period-averaged radiated power,

$$P = \frac{\omega}{2\pi} \iint p'_{bc} u'_{bc} \cdot d\mathbf{A} dt, \quad (5)$$

To differentiate between energy contained in fundamental and second harmonic internal tides, the velocity and pressure fields from simulation results are first fit to harmonic functions of the form:

$$[u(t), v(t), w(t), p(t)] = C + \sum_{n=1}^4 B_n \sin(n\omega t + \phi_n), \quad (6)$$

It is necessary to include terms at three and four times the tidal forcing frequency because motions at these frequencies are produced by nonlinear interactions between the ω and 2ω flow components, especially at higher tidal forcing amplitude. Equation (5) is evaluated separately for the fundamental and second harmonic internal tides using the $n = 1$ and $n = 2$ (respectively) parameters obtained from the fit to equation (6). The in-plane and out-of-plane second harmonics are reason-

ably distinct (see Figure 1c), but there is a small overlap due to the finite spatial extent of the wave beams. For simplicity, we consider second harmonic waves within 45° of the tidal forcing direction to be in-plane harmonics, with the out-of-plane second harmonics being defined outside these limits.

[16] At small tidal forcing amplitude, the power radiated as second harmonics is negligible. However, since the amplitude of the harmonic waves has a quadratic dependence on tidal forcing amplitude, their contribution to the wave field becomes significant with increasing forcing amplitude. At forcing amplitude $A/\sigma = 1$, 35% of the radiated power is in second harmonics, with 16% being radiated perpendicular to the forcing plane. These unexpected waves could be an additional source of mixing energy near bottom topography.

4. Discussion

[17] Existent models for internal wave generation do not include the possibility of the generation of internal tides perpendicular to the tidal forcing direction. However, we find strong perpendicular internal tides in our laboratory experiments and direct numerical simulations of tidal flow over a Gaussian mountain. For low tidal forcing amplitudes, the fraction of energy contained in internal tides in the out-of-plane direction is very small. However, at larger forcing amplitudes, corresponding to physical cases of large tidal excursion distance or small topography, the out-of-plane internal tides become significant. These perpendicular internal tides could affect parameterizations of internal tide generation in the ocean, especially in regions of small scale topographic roughness where the excursion parameter is large and nonlinear effects such as second harmonic generation become important. Indeed, Nycander [Nycander, 2005] has shown that 3D roughness and small topographic features on larger topography produce stronger internal tides than previously thought. Further, Muller and Buhler [2009] recently found that topographic features with horizontal length scales less than 10 km have a large effect on the presence of instabilities in the internal tides that are generated. These studies indicate that the large excursion parameter (large tidal forcing amplitude) regime could be more significant in the ocean than previously thought. As a result, a significant amount of the energy converted from barotropic to baroclinic tides can be generated perpendicular to the tidal forcing direction.

[18] **Acknowledgments.** We thank Frank Ham for access to the CDP numerical code. This research was supported by the National Science Foundation grant CBET-0755114. The Texas Advanced Computing Center (TACC) at The University of Texas at Austin provided high performance computing resources.

References

- Appleby, J. C., and D. G. Crighton (1987), Internal gravity-waves generated by oscillations of a sphere, *J. Fluid Mech.*, *183*, 439–450.
- Baines, P. G. (2007), Internal tide generation by seamounts, *Deep Sea Res., Part I*, *54*, 1486–1508.
- Balmforth, N. J., and T. Peacock (2009), Tidal conversion by supercritical topography, *J. Phys. Oceanogr.*, *39*, 1965–1974.
- Echeverri, P., M. R. Flynn, K. B. Winters, and T. Peacock (2009), Low-mode internal tide generation by topography: An experimental and numerical investigation, *J. Fluid Mech.*, *636*, 91–108.
- Egbert, G. D., and R. D. Ray (2000), Significant dissipation of tidal energy in the deep ocean inferred from satellite altimeter data, *Nature*, *405*, 775–778.
- Flynn, M. R., K. Onu, and B. R. Sutherland (2003), Internal wave excitation by a vertically oscillating sphere, *J. Fluid Mech.*, *494*, 65–93.
- Ham, F., and G. Iaccarino (2004), Energy conservation in collocated discretization schemes on unstructured meshes, annual research brief, Cent. for Turbulence Res., Stanford, Calif.
- Holloway, P. E., and M. A. Merrifield (1999), Internal tide generation by seamounts, ridges, and islands, *J. Geophys. Res.*, *104*, 25,937–25,951.
- Jayne, S. R., L. C. St. Laurent, and S. T. Gille (2004), Connections between ocean bottom topography and Earth's climate, *Oceanography*, *17*, 65–73.
- Khatiwal, S. (2003), Generation of internal tides in an ocean of finite depth: Analytical and numerical calculations, *Deep Sea Res., Part I*, *50*, 3–21.
- King, B., H. P. Zhang, and H. L. Swinney (2009), Tidal flow over three-dimensional topography in a stratified fluid, *Phys. Fluids*, *21*, 116601, doi:10.1063/1.3253692.
- Muller, C. J., and O. Buhler (2009), Saturation of the internal tides and induced mixing in the abyssal ocean, *J. Phys. Oceanogr.*, *39*, 2077–2096.
- Munk, W., and C. Wunsch (1998), Abyssal recipes ii: energetics of tidal and wind mixing, *Deep Sea Res., Part I*, *45*, 1977–2010.
- Munroe, J. R., and K. G. Lamb (2005), Topographic amplitude dependence of internal wave generation by tidal forcing over idealized three-dimensional topography, *J. Geophys. Res.*, *110*, C02001, doi:10.1029/2004JC002537.
- Nycander, J. (2005), Generation of internal waves in the deep ocean by tides, *J. Geophys. Res.*, *110*, C10028, doi:10.1029/2004JC002487.
- Peacock, T., P. Echeverri, and N. J. Balmforth (2008), An experimental investigation of internal tide generation by two-dimensional topography, *J. Phys. Oceanogr.*, *38*, 235–242.
- Petrelis, F., S. L. Smith, and W. R. Young (2006), Tidal conversion at a submarine ridge, *J. Phys. Oceanogr.*, *36*, 1053–1071.
- Zhang, H. P., B. King, and H. L. Swinney (2007), Experimental study of internal gravity waves generated by supercritical topography, *Phys. Fluids*, *19*, 096602, doi:10.1063/1.2766741.

B. King, H. L. Swinney, and H. P. Zhang, Center for Nonlinear Dynamics, University of Texas at Austin, 1 University Station C1600, Austin, TX 78712, USA. (bking@chaos.utexas.edu)